Measuring the Thermal Conductivity of Flowing Liquid Samples Using the Three Omega Method

Jonggan Hong
e-mail: poshjg@postech.edu

Dongsik Kim
e-mail: dskim87@postech.edu

Department of Mechanical Engineering,
POSTECH, Pohang 790–784,
Republic of Korea

The thermal conductivity of a liquid is generally measured under conditions that suppress bulk flow in the sample. However, in situ measurement of the thermal conductivity of a flowing liquid would be useful in various scientific and engineering applications. This work demonstrates that a thermal wave technique, such as the three omega method, can effectively measure the thermal conductivity of flowing liquid if the frequency range is adjusted such that the thermal boundary layer is sufficiently thinner than the momentum boundary layer. A new dimensionless number was defined to assess the convection effects, and a criterion for thermal conductivity measurements was obtained for water flowing in a circular tube. [DOI: 10.1115/1.4006384]

Keywords: convection, liquid, thermal conductivity measurement, thermal wave, three omega method

1 Introduction

A material's thermal conductivity is one of its important properties and is a measure of the ability to transport thermal energy by diffusion. Because thermal conductivity is defined by Fourier's law of heat conduction, the thermal conductivity of a liquid is generally measured in the absence of bulk flow. However, many important applications would find utility in an in situ measurement of the thermal conductivity of a flowing liquid sample. In various thermal sensors, such as hot wire anemometers [1,2], thermal accelerometers [3,4], pressure and vacuum gauges [5,6], liquid level sensors [7,8], and oil composition sensors [9], decoupling the thermal conductivity information from the convection effects may increase the sensor sensitivity or enable the extraction of additional information from the sensor signal. For example, during thermal sensing of a refrigerant-lubricant mixture's concentration in a refrigeration cycle, the thermal conductivity of the flowing liquid sample must be accurately measured while the liquid is flowing [9]. In addition to engineering applications, measuring the thermal conductivity of moving fluids would assist studies of the properties of unstable or chemically reactive liquids.

The 3ω method is an ac (alternating current) thermal technique used for measuring the thermal conductivity of a sample using propagation of thermal waves into the sample. It has been widely used to measure the thermal properties of thin films, bulk solids, or liquids [10–15]. Because the 3ω method involves shallow penetration of a thermal wave, it requires only a small volume of the sample [14,15]. Furthermore, flow effects can be reduced by decreasing the thermal penetration depth, i.e., by increasing the frequency range. In fact, we demonstrated measurement of the thermal conductivity of various liquids flowing in a microchannel, although the flow effect was relatively weak and the method required complicated numerical computation schemes for the inverse heat transfer problem [15]. In previous work on thermal liquid level sensing, we found that the ac thermal response was not significantly affected by the flow induced by magnetic stirring if the frequency was chosen appropriately [8].

Recently, Wang and Peterson [16] conducted a scaling analysis of the two-dimensional thermal wave propagation problem on a flat plate assuming a linear velocity profile ($u = cy$). They identified a new dimensionless parameter useful for describing the convection term, c/ω, which is the ratio between the flow velocity gradient and the operating frequency. Numerical simulation results showed that the temperature signal could be used to measure flow properties near a surface, for example, the wall shear stress.

For the thermal wave problem with a laminar flow in a circular tube, a dimensionless number $U_0/R\omega$ can be considered by assuming a linear velocity profile as in Wang and Peterson's work [16]. The number can be interpreted as a modified Wang and Peterson number obtained by substituting $c = U_0/R$ into the Wang and Peterson number c/ω. Accordingly, use of the dimensionless number for an internal-flow thermal-wave problem can be justified only when the velocity profile within the thermal penetration region is linear. The laminar flow in a circular pipe of radius R has a parabolic velocity profile $[u = 2U_0(1 - r^2/R^2)]$ and the thermal-wave penetration $\sim\sqrt{\alpha/2\omega}$ can be adjusted not to exceed $0.1R$ in our problem. In this narrow heat-affected zone $(0.9R < r < R)$, the velocity profile can be approximated by a linear profile whose slope is taken at $r = R$, i.e., $-du/dr|_{r=R} = 4U_0/R$. The maximum deviation that can be caused by using the linear profile is less than 5.3%. It is thus reasonable to use the dimensionless number $U_0/R\omega$, neglecting the factor 4, as a parameter to assess the convection effect on measuring the thermal conductivity of the flowing liquid. Consequently, this work examined the effects of liquid flow on the 3ω method using numerical calculations and experiments, and the results were analyzed based on the dimensionless number $U_0/R\omega$, showing that the dimensionless number can serve as an effective criterion to assess the flow effect.

2 Numerical Calculations

Solutions to transient heat transfer problems with periodic boundary conditions can be obtained by variation of parameters or by superposition [17,18]. A complete solution to the problems can be divided into a periodic, sustained solution and a transient solution. As the transient response decays as time increases, only the sustained part can be considered after a critical time, as in this work. In this case, the complex combination method can be employed to obtain the sustained solution. To apply the complex combination method, the governing equation and boundary condition must be linear and homogenous except for the nonhomogeneous periodic boundary condition [17,18].

In the present work, a line heater was placed on the bottom of the tube and heated periodically to generate thermal waves that propagated into a liquid flowing in a circular tube (Fig. 1). In the absence of internal heat generation or viscous dissipation, the energy equation under constant thermal properties can be expressed by

$$\alpha\nabla^2 T = \frac{\partial T}{\partial t} + \vec{v}\cdot\nabla T \tag{1}$$

Equation (1) is homogenous, but the convection term, the second term on the right hand side, is nonlinear. However, if we assume a simple laminar velocity profile in which the velocity components are functions of position only as

$$u = 2U_0\left(1 - \frac{r^2}{R^2}\right) = 2U_0\left(1 - \frac{x^2 + y^2}{R^2}\right) \tag{2}$$

Contributed by Applied Mechanics of ASME for publication in the JOURNAL OF HEAT TRANSFER. Manuscript received March 15, 2011; final manuscript received March 12, 2012; published online June 27, 2012. Assoc. Editor: Oronzio Manca.

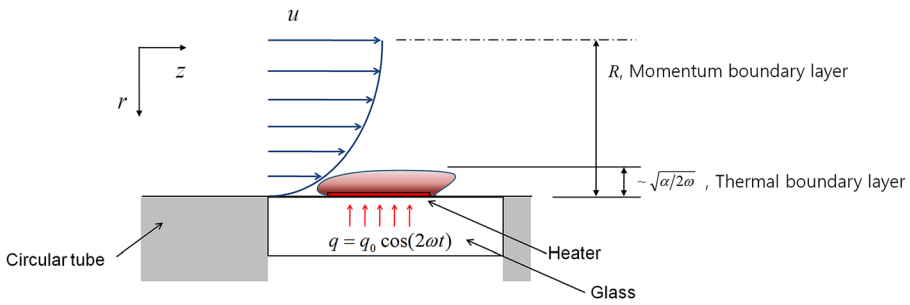

Fig. 1 Schematic diagram illustrating the thermal wave problem in a circular tube

the velocity field becomes decoupled from Eq. (1). Accordingly, Eq. (1) becomes linear and homogeneous.

Application of an alternating current (ac) of frequency ω to a heater generates Joule heating at a frequency of 2ω. The heat flux boundary condition has both a constant heating part and a periodic heating part. The constant heat flux causes only a steady temperature increase (a dc offset) in the temperature field once the periodic condition is reached. The sinusoidal heat flux generates the temperature oscillation which is employed in the 3ω method. Because the 3ω method uses the frequency dependence of temperature oscillations, the dc offset by the constant heat stimulus is not needed to find the thermal properties of a sample. Changes in thermal properties by the steady temperature increase could affect the temperature oscillations, but the effect was negligible under the low-power heating condition of the 3ω method. Thus, the effect of the constant heat source is ignored in the theory on the 3ω method [10–13]. Also, it is noted that the complex combination method can be used when the periodic boundary condition is sinusoidal, proportional to a sine or cosine function [17,18]. For simplicity, therefore, the boundary condition is assumed as

$$-\vec{n}\cdot(-k\nabla T)|_{\text{heater surface}} = q_0\cos(2\omega t) \tag{3}$$

Consequently, the complex combination method can be applied with the above-mentioned assumptions. A complex exponential solution is assumed for the temperature as

$$T = \tilde{T}\exp(i2\omega t) \tag{4}$$

Substituting Eq. (4) into Eq. (1) gives

$$\alpha\nabla^2\tilde{T} = i2\omega\tilde{T} + \vec{v}\cdot\nabla\tilde{T} \tag{5}$$

Adding the periodic condition which is out of phase by $\pi/2$ with the original one to Eq. (3) gives

$$-\vec{n}\cdot(-k\nabla\tilde{T})|_{\text{heater surface}} = q_0 \tag{6}$$

The solution to the new differential equation (Eq. (5)) and boundary condition (Eq. (6)) is the temperature response to the periodical heating in the sustained part of the complete solution.

Three-dimensional numerical calculations based on the finite element method were conducted to reveal the effects of convection on the temperature of the heater. Computational domains were divided into polycarbonate, liquid, and glass domains (Fig. 2). Three different-sized liquid domains whose diameters $D = 2.2$, 5, and 10 mm were used. The sizes of the other domains (A, B) were selected to be large enough to surround the liquid domain. The partial differential equation (Eq. (5)) was used as the governing equation. Liquid flow in the liquid domain was assumed to be decoupled with the governing equation and to have a parabolic velocity profile for the fully developed laminar regime as Eq. (2) because most of our experimental results were obtained in the laminar regime and the turbulent regime is not our major concern. Reynolds number, Re_D, based on U_0 was chosen not to exceed 2100, and heating frequencies of 1, 10, and 100 Hz were used. The thermal mass of the thin-film heater in the 3ω method was neglected. Instead, a heat flux boundary condition with a size of 1 mm × 20 μm was set at the position of the heater. Equation (6) was applied as the heat flux boundary condition ($q_0 = 100$ kW/m^2) and the temperatures at all boundaries except the heat flux boundary were set to zero. To figure out the influence of variation of thermal properties, water and ethanol were chosen as flowing liquids in the liquid domain. Thermal analysis for water

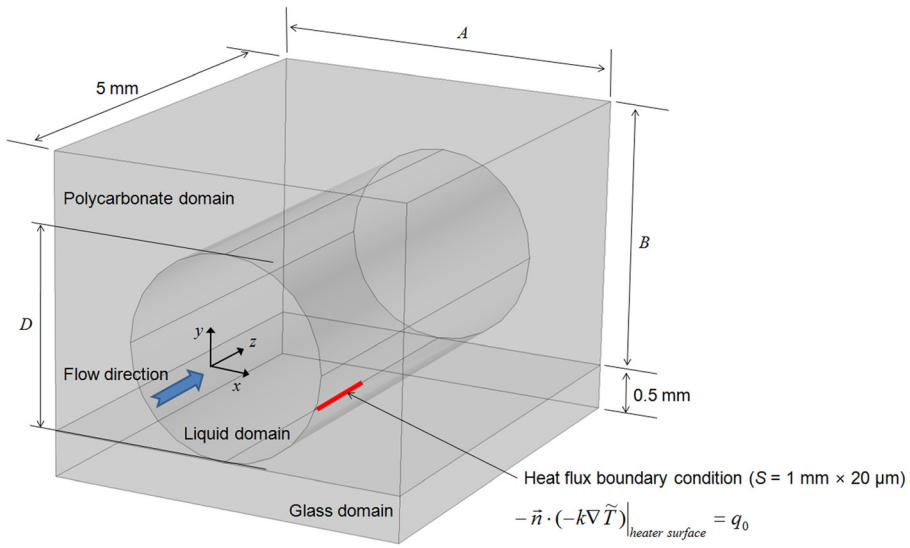

Fig. 2 Computational domains for numerical simulation

Table 1 Thermal properties used for the numerical calculations

	Thermal conductivity[a] ($W \cdot m^{-1} \cdot K^{-1}$)	Volumetric heat capacity[a] ($J \cdot m^{-3} \cdot K^{-1}$)
Water	0.607	4.17×10^6
Ethanol	0.169	1.93×10^6
Polycarbonate (tube)	0.201	1.40×10^6
Glass	1.10	2.6×10^6

[a]Data from Ref. [19].

and ethanol would cover most of the thermal property range of typical liquids (Table 1). It was assumed that the thermal properties were constant and no thermal resistances at the interfaces existed. The temperature response to periodical heating decays so rapidly that the heat transport phenomenon occurs near the heat flux boundary, only. Thus, a nonuniform tetrahedral mesh was structured with elements closely packed near the heat flux boundary. Solving Eqs. (5) and (6) by the numerical calculation gave the complex temperature field containing the real and imaginary parts (the amplitude and phase information) of the temperature oscillation produced by periodical heating. To obtain the temperature of the heater, the average temperature oscillation of the heat flux boundary was calculated.

3 Experiment

When the thermal conductivity of the liquid sample is measured using the 3ω method [8,9,12–15], flow of the liquid should be suppressed because a pure conduction problem is assumed. The flow effect on the 3ω method has been considered in the previous works [8,14,15]. The natural convection effect was neglected by setting the Rayleigh number to be smaller than the onset of natural convection ($Ra = 10^6$–10^9) [14]. The weak forced internal flow of various liquids in a microchannel did not affect the sensor signal significantly [15]. In an application of the 3ω method as a liquid level sensor [8], it was qualitatively shown that the forced external flow effect of magnetic stirring could be reduced by increasing the heating frequency, which reduced the thermal penetration depth. However, it was difficult to analyze and quantify the rotating flow field produced by the magnetic stirring. In the present work, to assess the flow effect quantitatively and measure the thermal conductivity of the flowing liquid, the sensor based on the 3ω method was applied to the inner wall of circular tubes in which water flowed.

The 3ω method needs a thin-film heater patterned on a substrate (Fig. 3). A 200 nm thick Au film and a 20 nm thick Cr film were deposited on a glass substrate and patterned by the lift-off process. The width and length of the heater were 20 μm and 1 mm, respectively. The single metallic strip acts as both a heater and a sensor by the following procedure. A sinusoidal current of angular frequency ω is supplied to the line heater, causing a temperature fluctuation at 2ω, which is related to the thermal properties of the substrate and the fluid contacting the heater, and to the heater geometry. The oscillating temperature perturbs the heater resistance at 2ω, and consequently induces an oscillating voltage signal at 3ω [8–15].

Average temperature fluctuation $\hat{T}$ of the heater for various configurations of the heater and its surroundings in the 3ω method has been analytically obtained from a pure conduction problem using the Fourier transform method [10,14]. If the thermal penetration depth $\sim\sqrt{\alpha/2\omega}$ is much larger than the half-width of the heater (10 μm), the solution can be expressed in a simple asymptotic form. Using the simple form, the thermal conductivity of the liquid sample is obtained from the slope of the curve relating ln ω to $\hat{T}_{\text{real}}$ [10,14]

$$k_s + k_l = -\frac{P}{2l\pi}\frac{d\ln\omega}{d\hat{T}_{\text{real}}} \tag{7}$$

The typical experimental setup for the 3ω method was employed to obtain the 3ω voltage signal (Fig. 3). The data acquisition setup consisted of a potentiometer, two differential amplifiers, and a lock-in amplifier. The ac current of angular frequency ω was supplied from an internal source of the lock-in amplifier to the heater. The amplitude P of the heater power was 3.25 MW. The 3ω component of the signal was approximately 10^{-3} times the ω component, so the ω component was eliminated by adjusting the gain of a differential amplifier to achieve a good signal-to-noise ratio. The 3ω signal was measured by the third-harmonic detection mode of the lock-in amplifier. The real and imaginary parts (amplitude and phase information) of the 3ω voltage signal

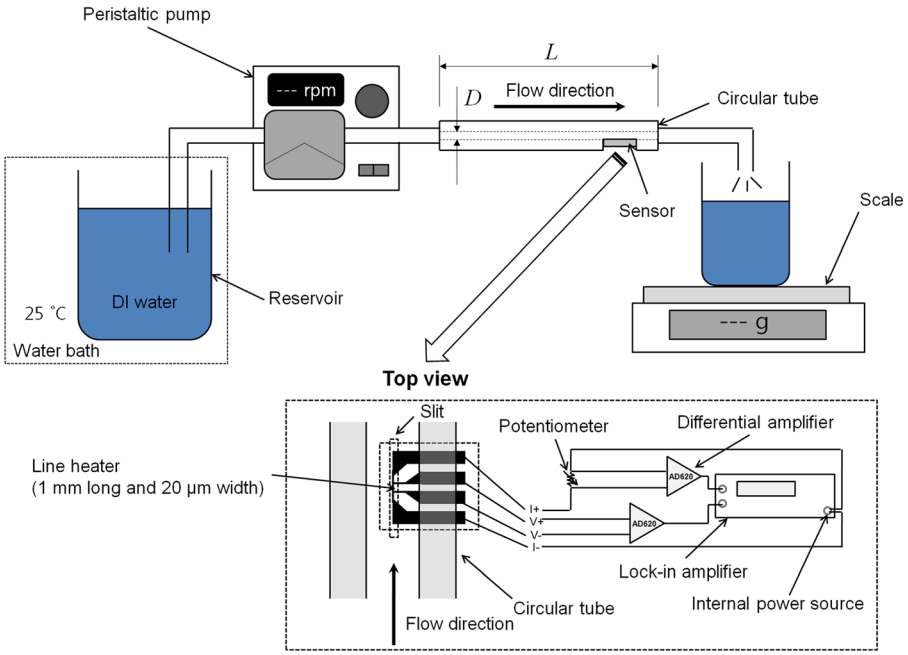

Fig. 3 Experimental setup

Table 2 Dimensions of the circular tubes

Model	D (mm)	L (mm)
#1	2.2	300
#2	3.2	440
#3	4.2	550

were collected repeatedly while varying the modulation frequency from 1.5 to 3263 Hz (19 data points). The voltage signal was converted to the corresponding temperature oscillation signal as

$$\hat{T} = \frac{2\hat{V}}{\gamma \lambda I} \tag{8}$$

The fabricated line heaters were calibrated by measuring the resistance change at temperature 25–35 °C in a water bath to obtain γ for Eq. (8). Depending on the sensor, γ varied slightly from 0.00256 to 0.00269 K^{-1}.

Among the acquired temperature signals over 1.5–3263 Hz, the upper bound of the frequency range for the slope method (Eq. (7)) was set to 12.7 Hz, as the thermal penetration depth into water is about 30μm at that frequency. The lowest frequency limit was 1.5 Hz, selected to avoid severe flow effects. The signals acquired over $f = 1.5$–12.7 Hz were used to measure the thermal conductivity.

An experimental setup for internal flow in three circular tubes was developed to analyze the effects of flow on thermal conductivity measurements using the 3ω method (Fig. 3). The circular tubes were made of polycarbonate and had three combinations of the length, L, and inner diameter, D, as listed in Table 2. The lengths of the tubes were selected such that the flow was fully developed at the position of the sensor. The length, L, was chosen to be larger than the entrance lengths, L_e, for laminar and turbulent flows [20]

$$\frac{L_e}{D} = 0.06\mathrm{Re_D} \text{ for laminar flow } (\mathrm{Re_D} < 2100) \tag{9}$$

$$\frac{L_e}{D} = 4.4(\mathrm{Re_D})^{1/6} \text{ for turbulent flow } (\mathrm{Re_D} > 4000) \tag{10}$$

A slit was cut in the circular tubes within which the line heater was installed so that it was exposed to the internal flow. A peristaltic pump was used to force water flow from a reservoir into the tube. It delivered flow rates from 0.9 to 565 ml/min during measurements. The motor speed of the peristaltic pump, controlled by a rotary encoded switch, was adjusted from 1 to 600 rpm. Mass flow rate was measured using an electronic scale and a timer. The increased mass for 10 s of flow was measured five times per measurement with a maximum random error 2% about the mean. The mass flow rate was converted to a volumetric flow rate with the density of water (997 kg/m^3 at 25 °C). The mean velocity, U_0, was calculated by dividing the flow rate by cross-sectional area of tubes. The mean velocities, U_0, were found to fall in the ranges 4.11 mm/s–2.47 m/s (11 data points) for $D = 2.2$ mm, 1.94 mm/s–1.16 m/s (12 data points) for $D = 3.2$ mm, and 1.13 mm/s–0.68 m/s (12 data points) for $D = 4.2$ mm. The maximum Reynolds numbers were 4852 at $D = 2.2$ mm, 3314 at $D = 3.2$ mm, and 2550 at $D = 4.2$ mm. The temperature signals were measured under the above-described flow conditions and the thermal conductivity of the flowing water was obtained using Eq. (7). All the measurements were conducted after waiting more than an hour for the water temperature to stabilize at 25 °C in a water bath.

The uncertainty of the experiment was analyzed using the method suggested by Beckwith et al. [21]. Precision uncertainty can be revealed with repeat-sampled data using statistical methods. The sensor was tested using several reference liquids (deionized water, ethanol, and ethylene glycol) in the absence of flow. Each sample was measured ten times. The experimental data were assumed to have the Gaussian distribution and precision errors of $\hat{T}$ and k were obtained as 0.2% and 0.5%, respectively, at a 95% confidence interval. During measurements for flowing water, the precision errors of $\hat{T}$ and k slightly increased to 0.6% and 0.9%, respectively. Known bias uncertainties were based on calibration accuracy of each equipment or experience [21]. Thus, the bias error was not affected by the flow condition. The bias uncertainties of each measured parameter are shown in Table 3, along with the equipment used to measure each parameter. Based on Eqs. (7) and (8), the temperature signal and thermal conductivity were expressed as functional forms

Table 3 Experimental bias uncertainties

Parameter	Bias uncertainty, W	Measuring equipment
λ	±0.05%	Agilent/34401A digital multimeter
I	±0.2%	Stanford research systems/SR810 DSP lock-in amplifier
γ	±1.0%	Agilent/34401A digital multimeter, K-type thermocouple
$\hat{V}$	±0.2%	Stanford research systems/SR810 DSP lock-in amplifier
ln ω	±0.003%	Stanford research systems/SR810 DSP lock-in amplifier
l	±0.5%	Olympus/BH2-UMA microscope

$$\hat{T} = f(\lambda, \hat{V}, I, \gamma) \tag{11}$$

$$k = f(\lambda^2,\ I^2,\ \gamma,\ \hat{V},\ \ln\omega,\ l) \tag{12}$$

As $\hat{T}$ and k are multiplicative functions of the parameters, the fractional bias uncertainties can be combined in an rms sense with weighting factors as

$$W_{\hat{T}} = \sqrt{W_\lambda{}^2 + W_{\hat{V}}{}^2 + W_I{}^2 + W_\gamma{}^2} \tag{13}$$

$$W_k = \sqrt{(2W_\lambda)^2 + (2W_I)^2 + W_\gamma{}^2 + W_{\hat{V}}{}^2 + W_{\ln\omega}{}^2 + W_l{}^2} \tag{14}$$

$W_{\hat{T}}$ and W_k were estimated to be 1.0% and 1.2%. A total uncertainty was estimated by taking the root-mean-square value of the bias and the precision uncertainties. When the liquid samples were still, the total uncertainty of $\hat{T}$ and k was 1.0% and 1.3%, respectively. In the presence of the water flow, the increased precision error slightly increased the total uncertainty, compared with that for the still liquids. Consequently, during measurements for flowing water, the total uncertainty of $\hat{T}$ and k was 1.2% and 1.5%, respectively.

The 3ω method was a powerful ac thermal technique to detect a weak thermal signal because the sensor signals at a specific heating frequency were selectively acquired by the lock-in amplifier. The short thermal penetration depth of periodical heating had the advantage of avoiding the flow effect. Additionally, the simple structure consisting of a single line heater on a substrate was proper for installation in the circular tube.

4 Results and Discussion

Figure 4 showed typical numerical results describing the effects of flow on the real part of the temperature oscillation. In the figure, cross-sectional views of the three-dimensional temperature distribution were observed at $f = 1$ Hz as the velocity of water changed. Because the thermal penetration depth in water was substantially smaller than the tube diameter, about 150 μm at 1 Hz, the thermal wave was confined to the vicinity of the wall. Once $U_0/R\omega$ was increased from 0 (Fig. 4(*a*)) to 80 (Fig. 4(*b*)), the temperature distribution was found to be disturbed by the flow. The complex temperature fluctuation $\tilde{T}$ at the heater surface (the heat flux boundary) was averaged to acquire $\hat{T}$. The real part of the average temperature, $\hat{T}_{\mathrm{real}}$, of the heater decreased from 1.396 to 1.275 K (9.1% decrease) due to convection effects.

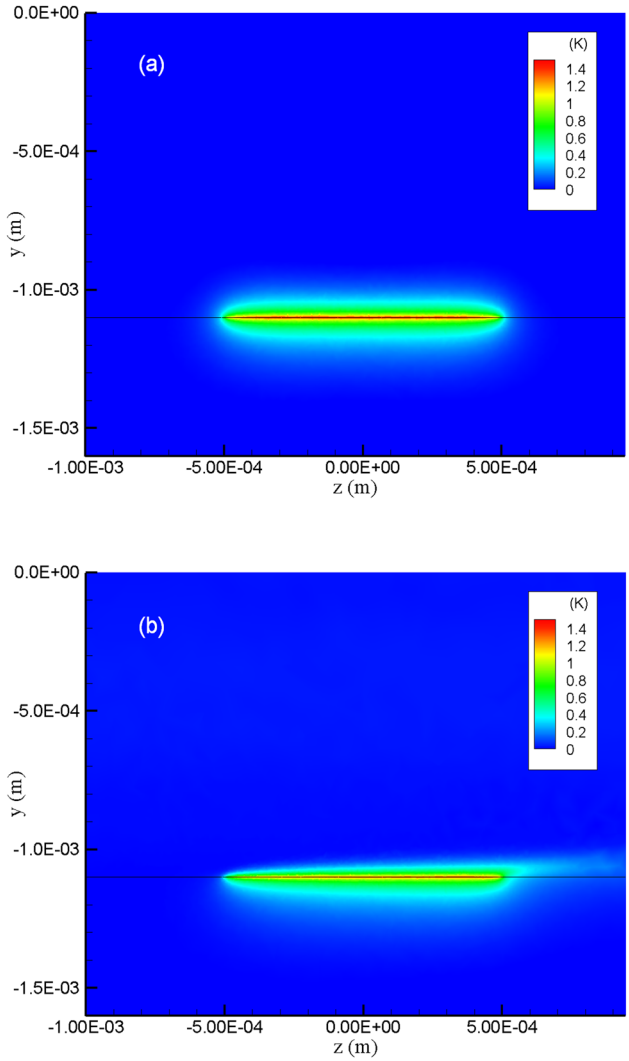

Fig. 4 Numerical results of the real part of the temperature oscillation: $D = 2.2$ mm, heating frequency = 1 Hz, and mean velocity U_0 of water = (*a*) 0 and (*b*) 0.55 m/s

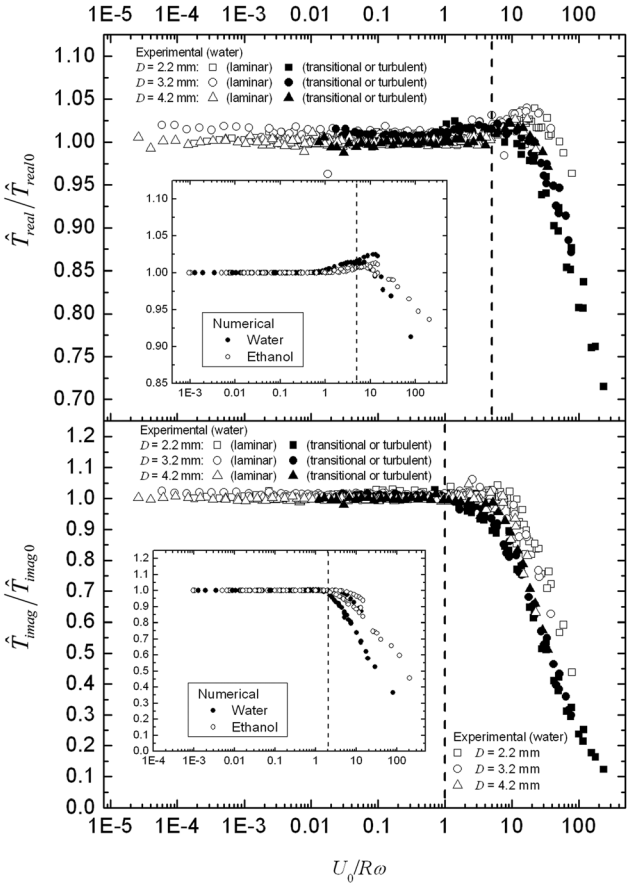

Fig. 5 Correlation between the dimensionless number describing the convection effects and the sensor signals

Computational results (210 data combinations of U_0, R, and ω for water and ethanol) and experimental results (665 data combinations of U_0, R, and ω for water) were plotted to reveal a correlation between the dimensionless number $U_0/R\omega$ and the sensor signal (real and imaginary parts of the temperature oscillations) (Fig. 5). The real and imaginary parts of the average temperature of the heater ($\hat{T}_{real}$ and $\hat{T}_{imag}$) were normalized by the corresponding values ($\hat{T}_{real0}$ and $\hat{T}_{imag0}$) obtained without the flow effect ($U_0 = 0$) at the same D and ω. The ranges of $\hat{T}_{real0}$ and $\hat{T}_{imag0}$ were 0.14–2.14 K and 0.14–0.50 K, respectively, depending on the heating frequency. In the laminar flow regime, the experimental results for water agreed reasonably well with the numerical results. For example, the effects of flow on the real part of the temperature signal were smaller than 1.5% for $U_0/R\omega < 5$ in both the experimental results and the numerical results. In the case of the imaginary part, the flow effects were smaller than 1.5% for $U_0/R\omega < 1$ in the experimental results and $U_0/R\omega < 2$ in the numerical results. Most experimental data approached unity, i.e., the theoretical prediction, as $U_0/R\omega$ decreased. However, in the case of $D = 3.2$ mm, $\hat{T}_{real}/\hat{T}_{real0}$ showed a relatively large bias from 1 even at low $U_0/R\omega$. We believe that the uncertainty in the measurement of the normalization factor $\hat{T}_{real0}$ in the high-frequency region (>1 kHz) caused the bias. This is due to the weak thermal response. The real part of the signal, which was used for measuring k, was less sensitive to the flow than the imaginary part. The imaginary part started to be affected by the convection effect at a lower $U_0/R\omega$ than the real part. Also, the imaginary part was attenuated by the convection much more strongly, decaying to almost zero.

Regardless of the flow regime, the flow effect started to appear at the similar value of $U_0/R\omega$ (Fig. 5). Also, the sensor signals in the transitional or turbulent flow regime decreased more than those in the laminar flow regime, after $U_0/R\omega$ exceeded the critical value. The numerical results for ethanol showed a quite similar trend with those of water, but the temperature change by the flow effect was less severe. It is believed to be due to the small thermal conductivity and heat capacity of ethanol compared to those of water. Also, the experimental data showed that changing U_0, ω, or R at a fixed $U_0/R\omega$ value did not affect the results significantly as long as the flow regime did not change. Although the proposed dimensionless number could not explain the magnitude difference of the temperature change by variation of the flow regime and thermal property of the liquid, $U_0/R\omega$ was found to be a good criterion to indicate the emergence of the flow effect.

The experimental results showed that at $U_0/R\omega \approx 5$, the real part of the signal began to deviate from the static value and then decrease dramatically due to convection. Because the real part of the signals acquired over the frequency range of 1.5–12.7 Hz was used for measuring k and the flow effect at 1.5 Hz was strongest, the less severe criterion $U_0/R\omega < 5$ at 1.5 Hz may be used to avoid flow effects. Using the real part of the temperature signal, the thermal conductivity of water flowing in the circular tubes was measured by increasing the mean velocity. The measured thermal conductivity was displayed with respect to the value of $U_0/R\omega$ at 1.5 Hz (Fig. 6). The apparent thermal conductivities were normalized by the static value ($k_0 = 0.607$ W/m·K at 25 °C). When $U_0/R\omega < 5$, the measured thermal conductivities agreed well with the

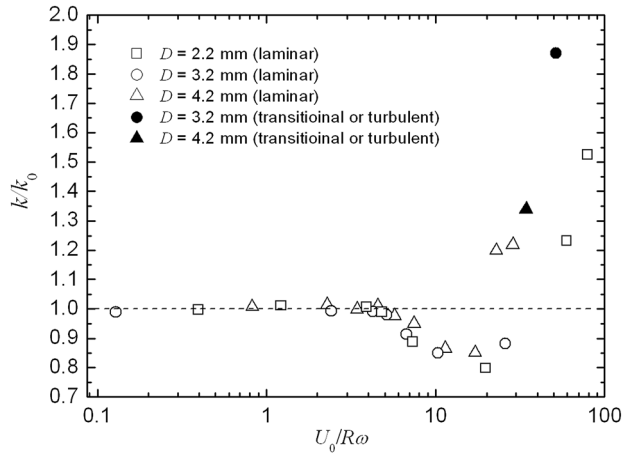

Fig. 6 Measurement of the thermal conductivity of water flowing in circular tubes

reference value measured without flow effects. The deviations were within ±2.3%. The thermal conductivity could be measured without a severe flow effect in the laminar regime. Although the flow effect was negligible even in the transitional or turbulent regime when $U_0/R\omega < 5$ (Fig. 5), over the fixed frequency range (1.5–12.7 Hz) for the slope method (Eq. (7)), the condition $U_0/R\omega < 5$ was not satisfied. Thus, the measured thermal conductivity in the transitional or turbulent regime severely deviated from the static value (Fig. 6).

Although the present work demonstrated successful measurement of the thermal conductivity of flowing water, the technique can be applied to other liquids if the flow condition and the heating frequency are properly adjusted. More specifically, the flow should be laminar and satisfy the conditions that $U_0/R\omega$ is small enough to neglect the flow effect and the velocity profile within the thermal penetration region is approximately linear. It is noted that the critical value of $U_0/R\omega$ to neglect the flow effect would be similar to what was found in this work (≈5) for other liquids because $U_0/R\omega$ is a universal parameter that determines the relative importance of the flow effect. Also, making the thermal penetration shallow by increasing ω to make the velocity profile approximately linear in the thermal boundary layer would not be difficult for many liquids whose transport properties are not substantially different from those of water.

5 Conclusions

The thermal conductivity of water flowing in a circular tube was successfully measured using the 3ω method, demonstrating the potential of the technique to measure the thermal conductivity of flowing liquid samples. When $U_0/R\omega < 5$, it was demonstrated experimentally that k of the flowing water could be measured using the real part of the thermal signal. The uncertainty of measuring k under the water flow condition was 1.5%. Deviations in k of flowing water with respect to the value of still water did not exceed ± 2.3%.

Acknowledgment

This work was supported by the Korean government (NRF-2011–0016489 and NRF-2011–0000109).

Nomenclature

c = velocity gradient, s^{-1}
f = heating frequency, Hz
i = imaginary unit
k = thermal conductivity, $W \cdot m^{-1} \cdot K^{-1}$
k_0 = thermal conductivity (no flow conditions), $W \cdot m^{-1} \cdot K^{-1}$
l = length of the heater, m
$\vec{n}$ = normal vector
q_0 = amplitude of the heat flux oscillation, $W \cdot m^{-2}$
r = radial coordinate, m
t = time, s
u = z-component of the velocity, $m \cdot s^{-1}$
$\vec{v}$ = velocity vector, $m \cdot s^{-1}$
x = x coordinate, m
y = y coordinate, m
z = axial coordinate, m
A = width of polycarbonate domain, m
B = height of polycarbonate domain, m
D = diameter of the circular tube, m
I = amplitude of input current oscillation, A
L = length of the circular tube, m
P = heating power, W
R = radius of the circular tube, m
Ra = Rayleigh number
Re_D = Reynolds number
T = temperature, K
$\tilde{T}$ = complex temperature oscillation, K
$\hat{T}$ = average temperature oscillation at the heater
U_0 = mean velocity of the flowing liquid, $m \cdot s^{-1}$
$\hat{V}$ = output 3ω voltage signal, V
W = fractional bias uncertainty, %

Greek Letters

α = thermal diffusivity, m^2/s
γ = temperature coefficient of resistance, K^{-1}
λ = resistance of the heater, Ω
ω = angular heating frequency ($= 2\pi f$), Hz

Subscripts

e = entrance length
imag = imaginary part
imag0 = imaginary part (no flow condition)
l = liquid
real = real part
real0 = real part (no flow condition)
s = substrate

References

[1] Durst, F., Al-Salaymeh, A., and Jovanovic, J., 2001, "Theoretical and Experimental Investigations of a Wide-Range Thermal Velocity Sensor," Meas. Sci. Technol., **12**, pp. 223–237.
[2] Chung, W. S., Kwon, O., Choi, D. S., Park, S., Choi, Y. K., and Lee, J. S., 2004, "Tunable AC Thermal Anemometry," Superlattices Microstruct., **35**, pp. 325–338.
[3] Mailly, F., Martinez, A., Giani, A., Pascal-Delannoy, F., and Boyer, A., 2003, "Design of a Micromachined Thermal Accelerometer: Thermal Simulation and Experimental Results," Microelectron. J., **34**, pp. 275–280.
[4] Courteaud, J., Crespy, N., Combette, P., Sorli, B., and Giani, A., 2008, "Studies and Optimization of the Frequency Response of a Micromachined Thermal Accelerometer," Sens. Actuators, A, **147**, pp. 75–82.
[5] Berlicki, T. M., 2001, "Thermal Vacuum Sensor With Compensation of Heat Transfer," Sen. Actuators, A, **93**, pp. 27–32.
[6] Kimura, M., Sakurai, F., Ohta, H., and Terada, T., 2007, "Proposal of a New Structural Thermal Vacuum Sensor With Diode-Thermistors Combined With a Micro-Air-Bridge Heater," Microelectron. J., **38**, pp. 171–176.
[7] Cantor, H. P., and Williams, O. M., 1976, "A Hot Wire Sensor for Liquid Level Detection," J. Phys. E, **9**, pp. 1136–1139.
[8] Hong, J., Chang, Y. S., and Kim, D., 2010, "Development of a Micro Liquid-Level Sensor for Harsh Environments Using a Periodic Heating Technique," Meas. Sci. Technol., **21**, p. 105408.
[9] Hong, J., Chang, Y. S., and Kim, D., 2011, "Development of a Micro Thermal Sensor for Real-Time Monitoring of Lubricating Oil Concentration," HVAC&R Res., **34**, pp. 374–382.
[10] Cahill, D. G., 1990, "Thermal Conductivity Measurement From 30 to 750 K: The 3" Method," Rev. Sci. Instrum., **61**, pp. 802–808.
[11] Cahill, D. G., Katiyar, M., and Abelson, J. R., 1994, "Thermal Conductivity of *a*-Si:H Thin Films," Phys. Rev. B, **50**, pp. 6077–6081.
[12] Moon, I. K., Jeong, Y. H., and Kwun, S. I., 1996, "The 3" Technique for Measuring Dynamic Specific Heat and Thermal Conductivity of a Liquid or Solid," Rev. Sci. Instrum., **67**, pp. 29–35.

[13] Chen, F., Shulman, J., Xue, Y., Chu, C. W., and Nolas, G. S., 2004, "Thermal Conductivity Measurement Under Hydrostatic Pressure Using the 3ω Method," Rev. Sci. Instrum., **75**, pp. 4578–4584.
[14] Choi, S. R., Kim, J., and Kim, D., 2007, "3ω Method to Measure Thermal Properties of Electrically Conducting Small-Volume Liquid," Rev. Sci. Instrum., **78**, p. 084902.
[15] Choi, S. R., and Kim, D., 2008, "Real-Time Thermal Characterization of 12 nl Fluid Samples in a Microchannel," Rev. Sci. Instrum., **79**, p. 064901.
[16] Wang, Z., and Peterson, R. B., 2010, "Thermal Wave Applications in Flow Fields With Steady Velocity Profile," ASME J. Heat Transfer, **132**, p. 054501.
[17] Myers, G. E., 1971, *Analytical Methods in Conduction Heat Transfer*, McGraw-Hill, New York.
[18] Poulikakos, D., 1994, *Conduction Heat Transfer*, Prentice-Hall, Englewood Cliffs, NJ.
[19] Lide, D. R., 2000, *CRC Handbook of Chemistry and Physics*, 81st ed., CRC Press, Boca Raton, FL.
[20] Munson, B. R., Young, D. F., and Okiishi, T. H., 1998, *Fundamentals of Fluid Mechanics*, 3rd ed., John Wiley & Sons, New York.
[21] Beckwith, T. G., Marangoni, R. D., and Lienhard, V. J. H., 1995, *Mechanical Measurements*, 5th ed., Addison-Wesley, New York.